ACS Catalysis

RESEARCH ARTICLE

pubs.acs.org/acscatalysis

# MFI Titanosilicate Nanosheets with Single-Unit-Cell Thickness as an Oxidation Catalyst Using Peroxides

Kyungsu Na,[†,‡] Changbum Jo,[†,‡] Jaeheon Kim,[†] Wha-Seung Ahn,[§] and Ryong Ryoo*[,†,‡]

[†]Center for Functional Nanomaterials and Department of Chemistry and [‡]Graduate School of Nanoscience and Technology (WCU) KAIST, Daejeon 305-701, Korea

[§]Department of Chemical Engineering, Inha University, Incheon 402-751, Korea

Supporting Information

**ABSTRACT:** Titanosilicate MFI (a three-letter structural code among ~200 zeolite framework codes) nanosheets of single-unit-cell thickness were synthesized with a diquaternary ammonium surfactant as the zeolite structure-directing agent, that is, $C_{16}H_{33}-N^+(CH_3)_2-C_6H_{12}-N^+(CH_3)_2-C_6H_{13}$. The resultant titanosilicate nanosheet possessed a large intersheet mesopore volume with high surface area due to the nanomorphic crystalline architecture as well as the isomorphically incorporated titanium species. Thus, it exhibited notable catalytic activities with high epoxide selectivity for bulky molecular epoxidation reactions using $H_2O_2$ or *t*-butyl hydroperoxide as an oxidant. In addition, the catalytic performance could be enhanced via postsynthetic fluoride treatment with $NH_4F$ that can reduce the surface silanol groups and, hence, increase the surface hydrophobicity.

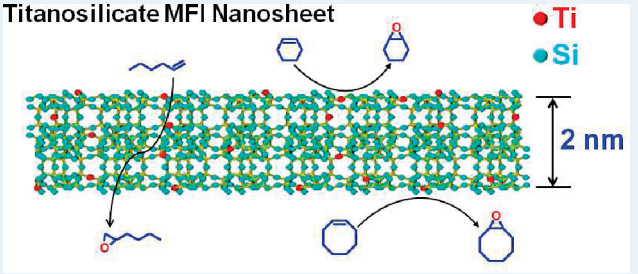


**KEYWORDS:** zeolite, MFI, titanosilicate, nanosheet, oxidation, catalyst, surfactant

## INTRODUCTION

Zeolite is a family of crystalline microporous molecular sieves, of which the frameworks consist of aluminum and silion atoms that are covalently bonded with oxygen atoms to form uniform micropores in a molecular dimension.[1−3] Zeolite structures can be determined according to the size, shape, and connectivity of the micropores. Such a distinct variability can specialize the zeolites to be used as a size-/shape-selective adsorbent, separation medium, and heterogeneous catalyst. Particularly in heterogeneous catalysis, zeolites are being currently used as one of the most important acid catalysts.[4−6] This is attributable to the benefit of the cation-exchange property of the aluminosilicate framework, the wide range of variability in the Si/Al ratio, and strong thermal/hydrothermal/mechanical stabilities.

In addition to the acid catalytic feature, zeolites can possess other catalytic functions, such as redox properties.[7−9] This can be achieved by isomorphically incorporating heteroelements such as transition metals into the framework instead of aluminum. Many types of zeolites possessing heteroelements inside the framework have been reported. For example, when the transition metals such as Ti or Fe are isomorphically incorporated into the silica framework, the resultant zeolites can exhibit a specific catalytic activity originating from a catalytic function of the transition metals.[10−13] Among them, titanosilicate zeolite, with a small fraction of titanium atoms incorporated into the silica framework, can exhibit high catalytic activity for oxidation reactions, including selective epoxidation of olefin molecules to epoxides.[10,11,14]

Titanosilicate TS-1 is the typical titanosilicate zeolite catalyst, having 10-membered oxygen ring (10MR) micropores in the MFI-type framework, which is a three-letter structural code of zeolite frameworks.[10,11,14] TS-1 is widely used as a highly selective and environmentally benign oxidation catalyst using $H_2O_2$ as an oxidant.[10,11,14] However, catalytic applications of this material are limited to small molecules that can diffuse into the 10MR micropore apertures. Bulkier substrates cannot be converted fluently within the micropores due to the steric constraint. Hence, considerable effort has been devoted to improving the diffusion efficiency of bulky substrates as well as smaller ones and, consequently, enhancement of the catalytic performance.[15−20]

Quite a large number of mesoporous titanosilicates, including Ti-MCM-41 and Ti-MCM-48, have been investigated for this purpose.[19,20] The mesoporous system with high external surface area is advantageous for diffusion of bulky substrates and their related catalysis. However, these types of materials are composed of noncrystalline frameworks.[21,22] Such noncrystalline silica frameworks are vulnerable to the water environment catalytic reaction condition, and hence, the catalytic recyclability is lower than the crystalline framework. The epoxidation activity of Ti in a disordered framework is also lower than the catalytic activity of tetrahedrally coordinated Ti in a crystalline zeolitic framework.[21] In addition, the mesopore walls are covered with a high concentration of silanol groups. The weakly acidic silanol groups usually cause epoxide ring-opening reactions. Although this problem can be significantly resolved by removing the silanols via silylation,[22,23] such vexatious treatment has obscured the wide catalytic use of mesoporous titanosilicate with noncrystalline framework.

Received: April 23, 2011
Revised: June 16, 2011
Published: June 17, 2011

Thin nanosheets of MWW and FER titanosilicate zeolites were reported during the past decade as efficient catalysts for the epoxidation of both small and bulky olefins using $H_2O_2$.[21,24] The high catalytic activity for bulky olefins indicated that the Ti sites on the external surface of the nanosheets could be more efficient catalytic sites than those on the Ti-MCM-41 mesopore walls. However, synthesis of such titanosilicate nanosheets was limited to zeolites that could be obtained as a 2-dimensional layered precursor. Thus, it remained unanswered whether the high catalytic activity was a specific property of Ti-MWW and Ti-FER or if it would be generalized in other Ti zeolites. The present work was undertaken in an attempt to answer this question, which may be useful in the design of other titanosilicate zeolite catalysts.

A new synthesis strategy for MFI zeolite nanosheets of a single-unit-cell crystal thickness was recently developed in the laboratory of the present authors by using a diquaternary ammonium surfactant with the formula $C_{22}H_{45}-N^+(CH_3)_2-C_6H_{12}-N^+(CH_3)_2-C_6H_{13}$ (designated $C_{22-6-6}$).[25−27] The MFI nanosheets thus synthesized were wide in the crystallographic $a-c$ plane and 2 nm thick along the $b$-axis. The nanosheets, in aluminosilicate or pure silica forms, could be obtained in a fully disordered assembly retaining a high intersheet mesopore volume after calcination. Accordingly, the nanosheet-type zeolites possessed numerous active sites on a wide external surface area and extremely thin diffusion pathway (2 nm along the $b$-axis). The nanosheet catalyst not only can exhibit high catalytic activity from small to bulky reactant molecules but also remarkably increased catalytic lifetime during the methanol-to-hydrocarbon conversion reaction. This was the first report of construction of a 2-dimensional architecture of three-dimensional MFI framework. In addition, this work demonstrated that the nanosheet-type ultrathin nanomorphic catalyst can be used as a valuable heterogeneous acid catalyst in various reactions.

Herein, the nanosheet synthesis method was extended to the preparation of titanosilicate zeolite in the MFI structure as an expoxidation catalyst. Due to the nanosheet-type ultrathin structure, the resultant titanosilicate nanosheet can possess a high external surface area and a large intersheet mesopore volume akin to the aluminosilicate MFI zeolite nanosheet. Thus, it can be used as a highly efficient epoxidation catalyst that can catalyze not only small linear olefins but also bulkier ones. In addition, a post-synthetic pathway to improve the catalytic performance of titanosilicate nanosheet zeolite was investigated in this work.

## RESULTS AND DISCUSSION

**Characterization of Materials.** Figure 1A shows powder X-ray diffraction (XRD) patterns of the TS-1 samples taken after calcination. The position of the XRD peaks of the nanosheet TS-1 is highly consistent with that of the bulk TS-1. Only the ($h0l$) reflections are predominant due to a considerable loss of long-range order along the $b$-axis. This occurs because the crystal growth along the $b$-axis is prevented by hydrophobic tails, as reported by Choi et al.[25] Growth is possible only to widen the $a-c$ plane. Line-broadening in the XRD peaks indicates that the nanosheet TS-1 is in the form of nanomorphic crystals. In addition, no indexable XRD peaks are observable in the low-angle region (Figure S1A in the Supporting Information), which implies that the nanosheet TS-1 is obtained as a disordered mesostructure in a unilamellar morphology. The $N_2$ adsorption isotherm in Figure 1B shows a very large mesopore volume for the nanosheet TS-1. The Brunauer−Emmett−Teller (BET) surface area and total pore volume of the nanosheet TS-1 after calcination are 580 $m^2\ g^{-1}$ and 0.61 $cm^3\ g^{-1}$, respectively. The mesopore diameter at the peak of distribution is 6.3 nm (Figure 1B inset). In contrast, in the case of bulk TS-1, the mesopore volume was negligible. The BET surface area and total pore volume are 393 $m^2\ g^{-1}$ and 0.21 $cm^3\ g^{-1}$, respectively. The micropore diameter of nanosheet TS-1 is determined by analyzing an Ar adsorption isotherm and subsequently converting it into a micropore size distribution according to nonlocal density functional theory. The result indicates that the micropore diameter (0.56 nm) of nanosheet TS-1 is exactly the same as that of bulk TS-1 composed of 10MR micropores (Figure S1B in the Supporting Information).

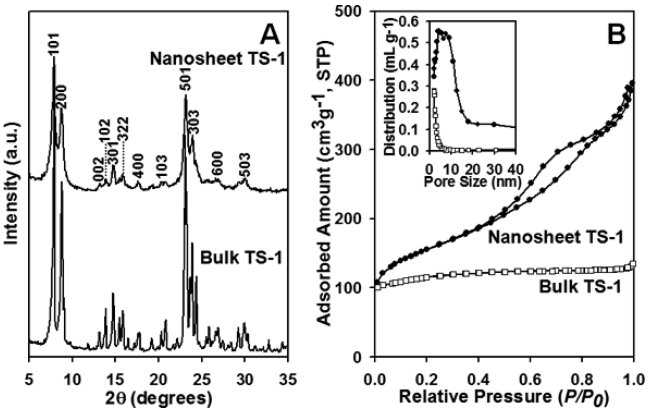


**Figure 1.** (A) XRD patterns, (B) $N_2$ adsorption isotherms and (B, inset) pore size distributions of nanosheet TS-1 and bulk TS-1.

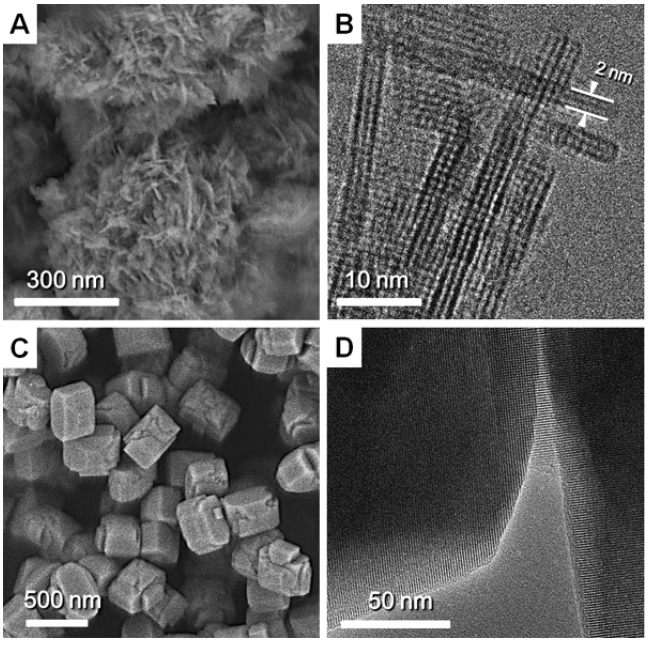


**Figure 2.** SEM (left column) and TEM (right column) of (A, B) nanosheet TS-1 and (C, D) bulk TS-1.

As shown in the scanning electron micrograph (SEM) images, the nanosheet TS-1 sample is obtained as a disordered assembly of thin plateletes (Figure 2A), whereas the bulk TS-1 is obtained as a single-crystalline morphology (Figure 2C). The morphology


dx.doi.org/10.1021/cs2002143 |ACS Catal. 2011, 1, 901–907

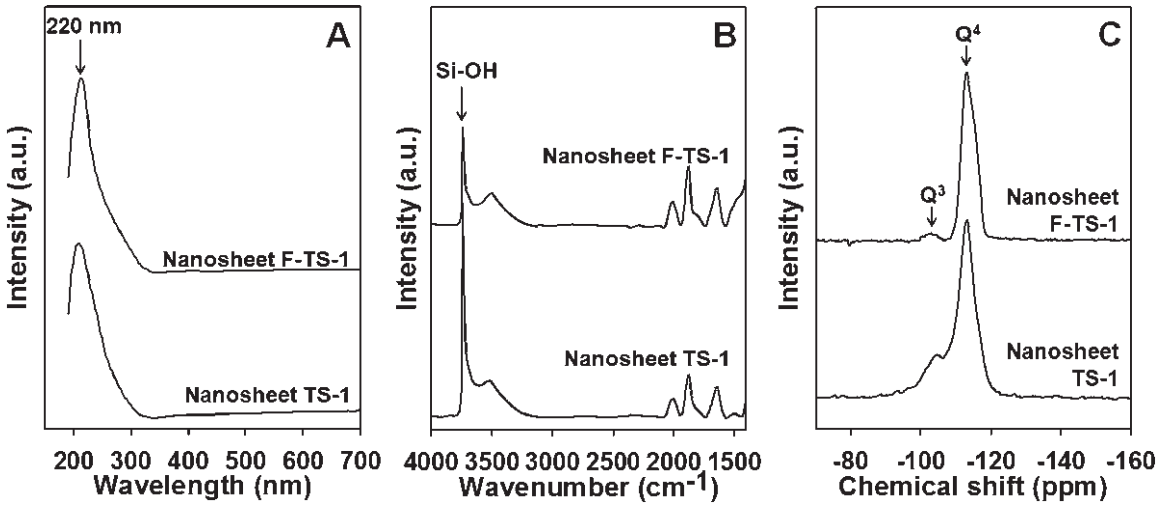


**Figure 3.** (A) DR-UV, (B) IR, and (C) $^{29}$Si MAS NMR spectra of nanosheet TS-1 before and after fluoride treatment. The nanosheet TS-1 after fluoride treatment is designated as nanosheet F-TS-1 in the above spectra.

**Table 1. Catalytic Activities of Titanosilicate Catalysts during the Epoxidation of Olefins Using $H_2O_2$ for 2 h at 60 °C**[a]

| | | | | olefin epoxidation results | | | | | | | | |
|---|---|---|---|---|---|---|---|---|---|---|---|---|
| | | | | 1-hexene | | | cyclohexene | | | cyclooctene | | |
| catalyst | Si/Ti[b] (ICP) | $S_{ext}$[c] ($m^2\ g^{-1}$) | $S_{BET}$[d] ($m^2\ g^{-1}$) | C[e] (%) | S[f] (%) | E[g] (%) | C (%) | S (%) | E (%) | C (%) | S (%) | E (%) |
| bulk TS-1 | 55 | 65 | 393 | 19.7 | 99 | 97 | 1.2 | 99 | 86 | 0.6 | 99 | 84 |
| Ti-MCM-41 | 61 | 835 | 861 | 1.5 | 71 | 72 | 9.8 | 14 | 74 | 6.6 | 74 | 71 |
| nanosheet TS-1 | 57 | 425 | 580 | 13.9 | 95 | 89 | 10.5 | 43 | 84 | 9.4 | 91 | 83 |
| nanosheet F-TS-1 | 54 | 405 | 558 | 12.8 | 95 | 81 | 25.0 | 69 | 87 | 15.3 | 95 | 86 |

[a] Reaction conditions: catalyst, 35 mg; olefin,12 mmol; $H_2O_2$, 3.3 mmol; acetonitril, 10 mL; 60 °C, 2 h. [b] Si/Ti mole ratio measured by inductively coupled plasma (ICP) atomic emission spectroscopy. [c] $S_{ext}$ is the external surface area calculated from the *t*-plot method. [d] $S_{BET}$ is the total surface area calculated from the BET method. [e] Conversion of olefin relative to the maximum possible (%). [f] Epoxide selectivity (%). [g] Oxidant efficiency = (amount used for olefin oxidation)/(amount used for olefin oxidation + amount decomposed) × 100 (%).

of nanosheet TS-1 is similar to the unilamellar MFI as reported previously.[25,27] The transmission electron micrograph (TEM) image in Figure 2B shows that the thickness of nanosheet TS-1 is only 2 nm, which corresponds to the lattice parameter of the *b*-axis. Intersheet mesopores are observable between neighboring nanosheets. In contrast, no mesopores exist in the bulk TS-1. Only small micropores are arranged with a long diffusion pathway in a single crystal.

The electronic state of Ti in the titanosilicate zeolites was examined by a diffuse-reflectance (DR) UV spectrometer. The narrow UV absorption band centered at 220 nm (Figure 3A) indicates that most Ti atoms in the nanosheet TS-1 are tetrahedrally coordinated inside the silica framework. No significant absorption at the 260 and 330 nm bands occurred in the UV analysis, which indicates extraframework Ti species are negligible. Since the nanosheet TS-1 is obtained as a nanomorphic crystal, the wide external surface should be terminated with a large number of silanol groups. This is evidenced by the sharp peak at 3747 $cm^{-1}$ in the IR spectrum, which corresponds to the stretching band of the hydroxyl group in the isolated silanol (Figure 3B). In addition, the medium intensity of the $Q^3$ peak at −102 ppm in the $^{29}$Si magic-angle-spinning (MAS) NMR spectrum (Figure 3C) can also support the presence of partially condensed silanol species. The relative $Q^3/Q^4$ ratio of the nanosheet TS-1 is about 1/3.1, which indicates that the number of silanol groups per total Si sites in the nanosheet TS-1 is ∼32%. In the case of bulk TS-1, the number of silanol groups would be negligibly small due to the very narrow external surface area compared with the total BET surface area.

**Catalytic Tests.** The catalytic activity of the nanosheet TS-1 for alkene epoxidation was tested in comparison with bulk TS-1 and Ti-MCM-41. As already characterized above, bulk TS-1 possessed solely micropores inside the large, single crystal. Thus, the BET surface area and total pore volume is smaller than the nanosheet TS-1 (Table 1). On the other hand, Ti-MCM-41 possessed a large amount of mesopore volume, with an average mesopore diameter of 3.4 nm and high external surface area on the mesopore wall (Table 1). The bulk TS-1 and Ti-MCM-41 contained tetrahedrally coordinated Ti species, similar to the nanosheet TS-1 (Figure S2 in the Supporting Information).

The catalytic reaction was performed by using either aqueous $H_2O_2$ or organic TBHP as an oxidant. Table 1 shows the catalytic epoxidation results when using $H_2O_2$ as an oxidant (see also Table S1 in the Supporting Information for the results using organic TBHP). When the reaction was performed with $H_2O_2$, the bulk TS-1 showed high conversion and selectivity for 1-hexene epoxidation after 2 h of reaction at 60 °C. After more than 60 h of reaction, the catalytic conversion was almost saturated, around


dx.doi.org/10.1021/cs2002143 |*ACS Catal.* 2011, 1, 901–907

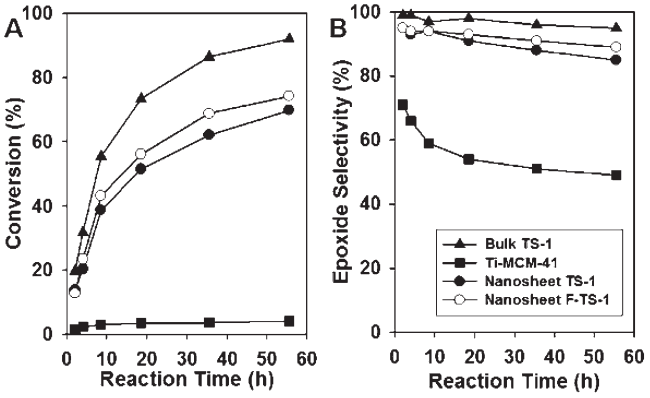


**Figure 4.** (A) Olefin conversion and (B) epoxide selectivity as a function of reaction time during 1-hexene epoxidation, using bulk TS-1, Ti-MCM-41, nanosheet TS-1, and nanosheet F-TS-1. (Reaction conditions: 35 mg of catalyst, 12 mmol of 1-hexene, 3.3 mmol of $H_2O_2$, 10 mL of acetonitrile, 60 °C).

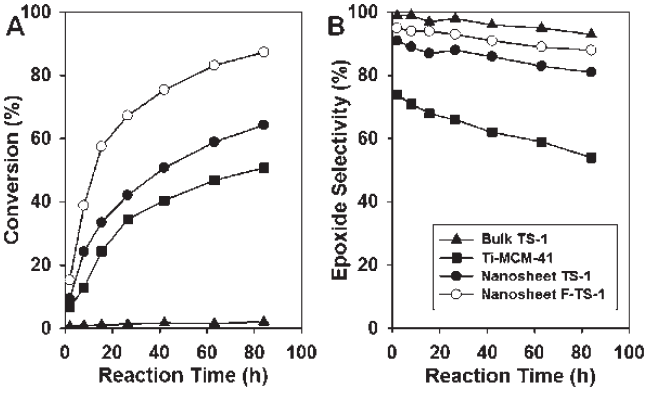


**Figure 5.** (A) Olefin conversion and (B) epoxide selectivity as a function of reaction time during cyclooctene epoxidation using bulk TS-1, Ti-MCM-41, nanosheet TS-1, and nanosheet F-TS-1. (Reaction conditions: 35 mg of catalyst, 12 mmol of cyclooctene, 3.3 mmol of $H_2O_2$, 10 mL of acetonitrile, 60 °C).

90%, due to the entire consumption of $H_2O_2$ via oxidation and slight decomposition (Figure 4A). In the case of bulky cyclic olefins (e.g., cyclohexene and cyclooctene), the conversion over bulk TS-1 was negligible. Even after much reaction time, the conversion did not increase (Figure 5A). This can be explained by the steric constraint of such bulky cyclic olefins to diffuse into the 10MR pore apertures.

In contrast, the nanosheet TS-1 exhibited high epoxidation catalytic activity for bulky cyclic olefins. Since the bulky cyclic olefins tested here were too big to approach the internal Ti sites, the high catalytic activity indicates that the Ti sites on the external surface of the nanosheet are sufficiently active to convert the bulky cyclic olefins to their epoxide counterparts. However, the conversion of cyclooctene was gradually saturated around 65% after 80 h (Figure 5A). Such saturation of olefin conversion is attributable to the presence of numerous weakly acidic silanol groups on the mesopore walls, which can cause $H_2O_2$ decomposition. The epoxide selectivity was somewhat low in the case of cyclohexene compared with other olefins. This can be explained in terms of the high strain in the resultant epoxide ring when it is linked to cyclohexane. This product is believed to transform into various side products due to the ring constraint of the epoxide structure in the cyclohexane.

In the case of 1-hexene, the nanosheet TS-1 showed 70% activity compared with the bulk catalyst (13.9% vs 19.7%), after 2 h at 60 °C (Table 1). Although the conversion increased gradually as a function of the reaction time (Figure 4A), the nanosheet TS-1 is still lower in 1-hexene conversion than the bulk TS-1. The lower conversion could be explained in terms of the different catalytic activity between external and internal Ti sites. Since 1-hexene could diffuse into the MFI micropores, the epoxidation reactions could fluently proceed not only on the external Ti sites, but also on the internal Ti sites. Here, in the case of bulk TS-1, the catalytic contribution of internal Ti sites on 1-hexene epoxidation would be very great due to the narrow external surface. If the catalytic activity of external Ti sites in nanosheet TS-1 is similar to that of internal Ti sites of bulk TS-1, the catalytic result over nanosheet TS-1 might be almost the same as the bulk TS-1. On this basis, it can be deduced that the Ti sites at the external surface are somewhat lower in catalytic activity than the internal ones. Nevertheless, the nanosheet catalyst was much better for 1-hexene epoxidation compared with Ti-MCM-41.

The Ti-MCM-41 exhibited epoxidation of 1-hexene of <3% after 2 h reaction due to the low catalytic activity of Ti sites on the amorphous wall and relatively low reactivity of linear olefins as compared with that of cyclic olefins.[28] For bulkier cyclic substrates, the Ti-MCM-41 exhibited catalytic conversion between the bulk and nanosheet TS-1. However, the epoxide selectivity and oxidant efficiency were very low. The low selectivity is attributable to the presence of numerous weakly acidic silanol groups on the mesopore walls, which are known to catalyze epoxide ring-opening reactions and cause $H_2O_2$ decomposition. On the other hand, bulk TS-1 has a very small external surface area. Hence, the silanol group content is too low to cause side reactions.

As reported in the literature, side reactions due to silanols on Ti-MCM-41 can be minimized using TBHP as an oxidant instead of aqueous $H_2O_2$.[22,23] This is because hydration of silanol groups causing poor olefin accessibility can be prevented in a $H_2O$-free condition using TBHP. The effect of using TBHP was investigated for the present nanosheet TS-1 (see Table S1 in the Supporting Information). The result shows significant improvements in both conversion and epoxide selectivity for bulky olefins. Silylation of Ti-MCM-41 is also well known as a means of minimizing the side reactions.[22,23] However, in the case of 1-hexene epoxidation over the nanosheet TS-1, there were no positive effects due to silylation (Table S2 in the Supporting Information). The epoxide selectivity was already very high (95%), even before silylation, and there was no further improvement by silylation. The catalytic activity was somewhat decreased, which was most likely due to the blocking of zeolitic pore mouths by surface silylation. This seems to obscure a facile accessibility of olefins to the catalytic sites.

**Effect of Post-Synthetic Fluoride Treatment on the Epoxidation Reactions.** Fluoride treatment is often used to increase the hydrophobicity of inorganic surfaces terminated with −OH groups by decreasing the hydrophilic −OH groups.[29,30] Although the presence of fluoride anions in epoxidation reactions is reportedly detrimental to the catalytic activity of titanosilicate catalysts,[31,32] fluoride anions in zeolite synthesis gel can sometimes be used to decrease the crystal defect sites and, hence, increase the epoxidation catalytic activity.[33] In the present work, we assessed the post-synthetic fluoride treatment of the nanosheet TS-1 to decrease the concentration of silanols, ultimately with the purpose of increasing


dx.doi.org/10.1021/cs2002143 |ACS Catal. 2011, 1, 901–907

the surface hydrophobicity and, hence, the catalytic activity. Fluoride treatment was performed with $NH_4F$ on an as-synthesized sample (i.e., containing $C_{16-6-6}$) to prevent structural collapse and alleviate the detrimental effect of fluoride anions on the active Ti sites. When we conducted the fluoride treatment with a calcined sample, the structure collapsed somewhat, and the catalytic activity decreased.

The IR analysis indicated that peak intensity at 3747 $cm^{-1}$ of the calcined nanosheet TS-1 decreased to 40% as compared with a calcined sample before fluoride treatment (Figure 3B). This indicated that the amount of silanols should be decreased. $^{29}Si$ MAS NMR also showed a significant decrease in the intensity of the −102 ppm peak (Figure 3C). This peak corresponded to tetrahedral Si atoms that were bonded to three −OSi− and one −OH. From the comparison of the relative $Q^3/Q^4$ ratios between the nanosheet TS-1 samples before/after fluoride treatment, approximately 40% of the silanol groups disappeared upon fluoride treatment. A very small decrease in BET surface areas after fluoride treatment is observable (Table 1 and Table S3 in the Supporting Information). No appreciable change in XRD patterns is observed, reflecting that the intrinsic structures of the nanosheet were almost fully retained (Figure S3 in the Supporting Information). To investigate the specific effect of fluoride treatment on the structural property, we analyzed the $NH_4F$-treated nanosheet sample (i.e., nanosheet F-TS-1) with $^{19}F$ MAS NMR; however, no appreciable signals originating from fluorine atoms were detected. This indicates that fluorine atoms did not exist on the nanosheet sample after fluoride treatment. Thus, it can be concluded that the decrease of silanols was attributed to the formation of siloxane bridge [i.e., $(SiO)_3Si-O-Si(OSi)_3$] by condensing between neighboring silanols. Since the fluorine atoms are often used as a mineralizing agent for zeolite crystallization during the hydrothermal treatment at high temperature (100 °C in the present work), $NH_4F$ treatment might induce a recrystallization process on the nanosheet surface. The IR and $^{29}Si$ NMR spectroscopic analyses in Figure 3 can indicate the decrease in silanols. The sharp peak at 3747 $cm^{-1}$ in the IR spectrum in Figure 3B decreased, which corresponds to the decrease in the terminal silanols on the external surface. The intensity of the $Q^3$ peak at −102 ppm in the $^{29}Si$ NMR in Figure 3C significantly decreased. In addition, the $Q^4$ peak was appreciably narrowed after fluoride treatment, indicating that the crystallinity of the nanosheet TS-1 was improved by reducing the number of silanol sites and thereby forming siloxane bridges.

The fluoride-treated nanosheet TS-1 (i.e., nanosheet F-TS-1) was tested in the epoxidation reactions. As shown in Table 1, the effect of fluoride treatment appeared differently for various olefins. For bulky cyclic olefins, the olefin conversion, epoxide selectivity, and oxidant efficiency increased after fluoride treatment. The positive effect of fluoride treatment can be explained in terms of the decrease in the silanol concentration. As analyzed above, since the surface of the nanosheet TS-1 becomes less hydrophilic by decreasing the silanol concentration via fluoride treatment, it becomes possible to increase olefin accessibility to the catalytic Ti sites and, consequently, increase the reaction rate. Indeed, the result was commensurate with our expectations. When we followed the cyclooctene epoxidation as a function of reaction time (Figure 4A), the reaction was faster over nanosheet F-TS-1 than over nanosheet TS-1. Such an increase in the reaction rate should be attributed to the increase in hydrophobicity on the external surface by fluoride treatment. Since the hydrophobic surface could allow the bulky cyclic olefins to approach the Ti sites more easily, the epoxidation reactions could be enhanced. In addition, epoxide products, which are relatively less hydrophobic than olefins, could be released from the reaction zone more quickly. This reduces the possibility that the epoxide ring will open, and hence, the epoxide selectivity can also be increased as compared with the selectivity before fluoride treatment.

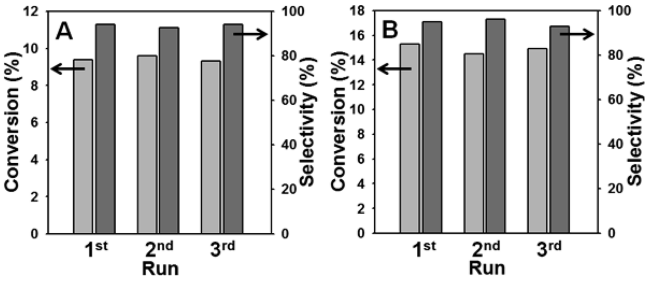


**Figure 6.** Recyclability tests of (A) nanosheet TS-1 and (B) nanosheet F-TS-1 during the cyclooctene epoxidation. (Reaction conditions: 35 mg of catalyst, 12 mmol of cyclooctene, 3.3 mmol of $H_2O_2$, 10 mL of acetonitrile, 60 °C 2 h).

In the case of 1-hexene, the effects of fluoride treatment on nanosheet TS-1 were insignificant as compared with the cyclic olefins. The conversion and reaction rate are very slightly improved after fluoride treatment (Table 1 and Figure 4B). Moreover, the catalytic activity of nanosheet F-TS-1 is still lower than that of bulk TS-1 due to the lower catalytic activity of external Ti sites as compared with that of the internal ones, as discussed in the previous section. Nevertheless, it is noteworthy that the catalytic activity of external Ti sites is sufficiently high to catalyze the internal alkenes, such as cyclic bulky olefins, with a relatively lower reactivity[28] as compared with the terminal alkene, such as 1-hexene.

When the fluoride treatment was performed on bulk TS-1, change in the catalytic activity and selectivity was negligible. This could be attributed to the catalytic contribution by the very narrow external surface of bulk TS-1 being negligible. Ti-MCM-41 was also treated with $NH_4F$, but the treatment rather decreased the catalytic activity. This was due to the structural collapse of noncrystalline silicate framework, as evidenced by XRD and $N_2$ adsorption analyses (Figures S3C and S4C in the Supporting Information).

## CONCLUSION

In conclusion, TS-1 nanosheets with 2-nm thickness were synthesized using the $[C_{16}H_{33}-N^+(CH_3)_2-C_6H_{12}-N^+(CH_3)_2-C_6H_{13}](OH^-)_2$ surfactant as an MFI zeolite structure-directing agent. On the basis of UV analysis and epoxidation of bulky and small olefins, it is concluded that the nanosheet TS-1 contained tetrahedrally coordinated Ti species with catalytic activities both inside the microporous framework and on the external surface. The catalytic activity of external Ti species is somewhat lower than that of internal ones. The activity of external Ti sites on nanosheet TS-1 is sufficiently high to catalyze the internal alkenes, such as cyclohexene and cyclooctene, due to their high reactivity as compared with the terminal alkene, such as 1-hexene. The conversion and epoxide selectivity were much better than those of Ti-MCM-41. Furthermore, the catalytic activity and epoxide selectivity of the external Ti sites for bulky cyclic olefins could be enhanced remarkably by reducing the amount of silanols via postsynthetic fluoride treatment. In addition, the nanosheet TS-1


dx.doi.org/10.1021/cs2002143 |ACS Catal. 2011, 1, 901–907

is recyclable at least three times without significant changes in their activity and epoxide selectivity (Figure 6). We conclude that the external surface of crystalline Ti-zeolite nanosheets, as exemplified by the present MFI and by previously reported MWW and FER, are much better as epoxidation catalysts using $H_2O_2$ and organic hydroperoxides than MCM-41-type Ti-containing ordered mesoporous materials composed of amorphous framework.

## EXPERIMENTAL SECTION

**Preparation of Materials.** The structure-directing surfactant having a diquaternary ammonium headgroup (i.e., $C_{16}H_{33}-N^+(CH_3)_2-C_6H_{12}-N^+(CH_3)_2-C_6H_{13}$ ($C_{16-6-6}$ for short)), was initially prepared in the bromide form by following the procedures outlined in the literature.[25−27] Prior to the synthesis of the zeolite, the bromide anions in the surfactant were ion-exchanged into hydroxide by using the column filled with anionic exchange resin (MTO-Dowex SBR LCNG OH form, Supelco). The ion-exchange procedure was repeated three times.

In a typical synthesis of a nanosheet TS-1, 0.01 mol of tetraethylorthosilicate (TEOS, TCI) was added to 10.8 mL of an aqueous solution containing 0.0007 mol of $C_{16-6-6}(OH)_2$. The mixture was magnetically stirred at room temperature until it became a homogeneous sol (for ∼10 min). This mixture was cooled in an ice bath, and a freshly prepared solution of 0.0002 mol of titanium(IV) butoxide (TBOT, Aldrich) in 0.003 mol of *n*-butyl alcohol was added dropwise. The resultant gel was further homogenized at 60 °C for 3 h under magnetic stirring. The molar composition of the final gel mixture was 100 $SiO_2$/7 $C_{16-6-6}(OH)_2$/2 $TiO_2$/6000 $H_2O$/30 *n*-butyl alcohol. The resultant gel was transferred to a Teflon-lined autoclave and hydrothermally crystallized at 140 °C under tumbling conditions (60 rpm). After a 10 day hydrothermal treatment, the zeolite product was filtered, washed with distilled water, and dried at 130 °C. The as-synthesized product was calcined at 550 °C for 3 h under air for surfactant removal or was used as-is for the postsurface fluorination process.

The bulk TS-1 and Ti-MCM-41 were prepared by following the literature.[10,20] For the investigation of the silylation effect on the nanosheet TS-1, postsurface silylation was performed by following the literature procedure.[23]

**Postsynthetic Fluoride Treatment.** Postsynthetic fluoride treatment of the titanosilicate samples was performed using the samples in the as-synthesized form before organic removal. In a typical treatment process, 0.3 g of the as-synthesized titanosilicate product was added to an aqueous solution containing $NH_4F$. The molar composition of the final mixture was 100 SiO/25 $NH_4F$/6000 $H_2O$. The temperature and time was varied according to the samples. For the bulk TS-1 and nanosheet TS-1, the fluoride treatment was performed at 100 °C for 12 h under tumbling conditions (60 rpm). In the case of Ti-MCM-41, the treatment was carried out at a lower temperature (∼70 °C). After the treatment, all the samples were filtered, washed rigorously with distilled water, and dried at 130 °C. Subsequently, the dried products were calcined at 550 °C for 3 h under air for organic removal before further characterization and catalytic use.

**Characterization.** Powder X-ray diffraction (XRD) patterns were measured with a Rigaku Multiflex diffractometer equipped with Cu $K_\alpha$ radiation (30 kV, 40 mA). $N_2$ adsorption isotherms were measured with a Micromeritics TriStar II volumetric adsorption analyzer at the liquid nitrogen temperature (77 K). Prior to the adsorption analysis, all samples were degassed under a vacuum for 12 h at 573 K. The surface area was calculated using the BET equation from adsorption data obtained $P/P_0$ values that were between 0.05 and 0.2. The external surface area was calculated by the *t*-plot method. The pore size distributions were analyzed from the adsorption branch of the isotherm using the Barrett−Joyner−Halenda algorithm. SEM images were taken at a low electron acceleration voltage in a gentle-beam mode (2 kV, Hitachi S-4800) without a metal coating, after mounting the samples on a carbon-coated tape. TEM images were obtained using a Tecnai G2 F30 at an operating voltage of 300 kV. The electronic state of the Ti in the titanosilicate samples was analyzed using a Jasco UV−vis spectrometer (V570) in DR mode. For the IR measurements, the titanosilicate samples were pressed to produce self-supported wafers (∼12 mg/cm$^2$) without binding agents. The samples were degassed at 400 °C for 2 h in an in situ IR cell. After cooling to room temperature, the IR spectra were measured by an FT-IR spectrometer (Bruker Vector 33) at room temperature with 40 scans and a resolution of 4 cm$^{-1}$. The $^{29}$Si solid-state MAS NMR measurements of the titanosilicate samples were performed using a Unity/Inova (Varian, 600 MHz) spectrometer operating at the designated frequencies of 119.182 MHz. The chemical shift for $^{29}$Si was referenced with respect to trimethylsilane. The $^{29}$Si NMR spectra were obtained under the following conditions: 2.0 $\mu$s pulse, 7 s relaxation delay, 15 kHz spinning rate, and 820 acquisitions. The NMR spectra were compared in the absolute intensity scale.

**Catalytic Reaction.** The catalytic reactions were performed using a Pyrex batch reactor (EYELA Chemistation) equipped with a reflux condenser. Typically, 35 mg of catalyst, 12 mmol of olefin, and 3.3 mmol of oxidant were added to 10 mL of acetonitrile. The olefin was varied with 1-hexene, cyclohexene, or cyclooctene, and the oxidant was varied with aqueous hydroperoxide (50 wt % $H_2O_2$ in water) or organic *t*-butyl hydroperoxide (5.5 M of TBHP in decane). All of the reagents were purchased from Aldrich and were used without further purification. The reactions were conducted at 60 °C for 2 h. The products were analyzed by gas chromatography equipped with a HP-1 capillary column (J&W Scientific; 30-m-long, 0.32-mm-i.d., and 0.25-$\mu$m-thick) and a flame ionization detector. The conversion of olefin was calculated on the basis of the amount of oxidant. The oxidant decomposition was determined by titration with 0.1 M $Ce(SO_4)_2$ of an aqueous solution. After the first catalytic reaction, the catalyst was recovered by filtration and washed with ethanol and acetone several times. The catalyst was dried at 130 °C and further calcined at 550 °C for 3 h under air before checking the catalytic recyclability.

## ASSOCIATED CONTENT

**Supporting Information.** Additional characterizations of materials and catalytic tests. This material is available free of charge via the Internet at http://pubs.acs.org/.

## AUTHOR INFORMATION

**Corresponding Author**

*Phone: (+82) 42-350-2830). Fax: (+82) 42-350-8130. E-mail: rryoo@kaist.ac.kr.

## ACKNOWLEDGMENT

This work was supported by the National Honor Scientist Program (20100029665) and World Class University Program

(R31-2010-000-10071-0) of the Ministry of Education, Science and Technology in Korea.

## REFERENCES


(1) Corma, A. *Chem. Rev.* **1997**, *97*, 2373.
(2) Cundy, C. S.; Cox, P. A. *Chem. Rev.* **2003**, *103*, 663.
(3) Cundy, C. S.; Cox, P. A. *Chem. Rev.* **2005**, *82*, 1.
(4) Corma, A. *Chem. Rev.* **1995**, *95*, 559.
(5) Tanabe, K.; Hölderich, W. F. *Appl. Catal., A* **1999**, *181*, 399.
(6) Rinaldi, R.; Schüth, F. *Energy Environ. Sci.* **2009**, *2*, 610.
(7) Sachtler, W. M. H.; Zhang, Z. *Adv. Catal.* **1993**, *39*, 129.
(8) Arends, I. W. C. E.; Sheldon, R. A.; Wallau, M.; Schuchardt, U. *Angew. Chem., Int. Ed.* **1997**, *36*, 1144.
(9) Schuchardt, U.; Cardoso, D.; Sercheli, R.; Pereira, R.; Cruz, R. S.; da Guerreiro, M. C.; Mandelli, D.; Spinacé, E. V.; Pires, E. L. *Appl. Catal., A* **2001**, *211*, 1.
(10) Thangaraj, A.; Eapen, M. J.; Sivasanker, S.; Ratnasamy, P. *Zeolites* **1992**, *12*, 943.
(11) Notari, B. *Adv. Catal.* **1996**, *41*, 253.
(12) Panov, G. I.; Sheveleva, G. A.; Kharitonov, A. S.; Romannikov, V. N.; Vostrikova, L. A. *Appl. Catal., A* **1992**, *82*, 31.
(13) Chu, C. T.-W.; Chang, C. D. *J. Phys. Chem.* **1985**, *89*, 1569.
(14) Reddy, J. S.; Kumar, R.; Ratnasamy, P. *Appl. Catal.* **1990**, *58*, L1.
(15) Camblor, M. A.; Corma, A.; Martínez, A.; Pérez-Paríente, J. *J. Chem. Soc., Chem. Commun.* **1992**, 589.
(16) Cheneviere, Y.; Chieux, F.; Caps, V.; Tuel, A. *J. Catal.* **2010**, *269*, 161.
(17) Fang, Y.; Hu, H. *Catal. Commun.* **2007**, *8*, 817.
(18) Tanev, P. T.; Chibwe, M.; Pinnavaia, T. J. *Nature* **1994**, *368*, 321.
(19) Corma, A.; Navarro, M. T.; Pérez-Paríente, J. *J. Chem. Soc., Chem. Commun.* **1994**, 147.
(20) Blasco, T.; Corma, A.; Navarro, M. T.; Pérez Pariente, J. *J. Catal.* **1995**, *156*, 65.
(21) Wu, P.; Nuntasri, D.; Ruan, J.; Liu, Y.; He, M.; Fan, W.; Terasaki, O.; Tatsumi, T. *J. Phys. Chem. B* **2004**, *108*, 19126.
(22) Igarashi, N.; Hashimoto, K.; Tatsumi, T. *Microporous Mesoporous Mater.* **2007**, *104*, 269.
(23) Fan, W.; Wu, P.; Tatsumi, T. *J. Catal.* **2008**, *256*, 62.
(24) Corma, A.; Diaz, U.; Domine, M. E.; Fornés, V. *J. Am. Chem. Soc.* **2000**, *122*, 2804.
(25) Choi, M.; Na, K.; Kim, J.; Sakamoto, Y.; Terasaki, O.; Ryoo, R. *Nature* **2009**, *461*, 246.
(26) Na, K.; Choi, M.; Park, W.; Sakamoto, Y.; Terasaki, O.; Ryoo, R. *J. Am. Chem. Soc.* **2010**, *132*, 4169.
(27) Na, K.; Park, W.; Seo, Y.; Ryoo, R. *Chem. Mater.* **2011**, *23*, 1273.
(28) van der Waal, J. C.; Rigutto, M. S.; van Bekkum, H. *Appl. Catal., A* **1998**, *167*, 331.
(29) Nur, H.; Hau, N. Y.; Misnon, I. I.; Hamdan, H.; Muhid, M. N. M. *Mater. Lett.* **2006**, *60*, 2274.
(30) Yamamoto, K.; Tsuji, M.; Washio, K.; Kasahara, H.; Abe, K. *J. Phys. Soc. Jpn.* **1983**, *52*, 925.
(31) Clerici, M. G.; Ingallina, P. *J. Catal.* **1993**, *140*, 71.
(32) Goa, Y.; Wu, P.; Tatsumi, T. *J. Phys. Chem. B* **2004**, *108*, 4242.
(33) Blasco, T.; Camblor, M. A.; Corma, A.; Esteve, P.; Guil, J. M.; Martínez, A.; Perdigón-Melón, J. A.; Valencia, S. *J. Phys. Chem. B* **1998**, *102*, 75.